# The Dependence of H-mode Energy Confinement and Transport on Collisionality in NSTX

S.M. Kaye[1], S. Gerhardt[1], W. Guttenfelder[1], R. Maingi[2]. R.E. Bell[1], A. Diallo[1], B.P. LeBlanc[1], M. Podesta[1]

[1] Princeton Plasma Physics Laboratory, Princeton University, Princeton, NJ 08543
[2] Oak Ridge National Laboratory, Oak Ridge, TN 37831

*E-mail contact of main author: kaye@pppl.gov*

**Abstract**. Understanding the dependence of confinement on collisionality in tokamaks is important for the design of next-step devices, which will operate at collisionalities at least one order of magnitude lower than in present generation. A wide range of collisionality has been obtained in the National Spherical Torus Experiment (NSTX) by employing two different wall conditioning techniques, one with boronization and between-shot helium glow discharge conditioning, and one using lithium evaporation. Discharges with lithium conditioning generally achieved lower collisionality. While differences in the confinement dependence on dimensional, engineering variables between the datasets differed, the various sets of data were unified by an underlying dependence on collisionality, exhibiting a strong increase of normalized confinement time with decreasing collisionality holding other dimensionless variables as fixed as possible. This result is consistent with gyrokinetic calculations that show microtearing and Electron Temperature Gradient modes to be more stable at lower collisionality. Ion transport, near neoclassical at high collisionality, became more anomalous at lower collisionality, possibly due to the growth of hybrid TEM/KBM modes in the outer regions of the plasma.

## 1. Introduction

Parametric dependences of plasma confinement and transport can be based on sets of dimensional parameters that can be controlled experimentally [1-3], or on dimensionless variables that are believed to represent more accurately the underlying physics mechanisms controlling transport [4, 5]. Examples of the former are plasma current, $I_p$, toroidal magnetic field, $B_T$, plasma density, $n_e$, and heating power, $P_{heat}$. The latter set of physics variables includes the normalized gyroradius, $\rho^* = \rho/a$, where $\rho$ is gyroradius and a is plasma minor radius, the plasma beta $\beta \propto p/B_T^2$, where p is plasma pressure, and the normalized collisionality, $\nu^* \propto n_e Z_{eff}/T_e^2$ for fixed q and geometry. The collisionality reflects the physics of both resistive and trapped particle effects. A recent review of the dependence of confinement on various dimensionless parameters [5] has, in fact, shown that by combining data from a range of devices, the collisionality dependence of normalized confinement, $B_T \tau_E$ where $\tau_E$ is energy confinement time, is itself a function of collisionality, with weaker dependences at lower $\nu^*$.

It is the purpose of this work to characterize and understand the causes of the collisionality dependence of plasma confinement in the high-power, low aspect ratio National Spherical Torus Experiment (NSTX). A large range of collisionality has been achieved in NSTX using various methods of wall conditioning. Early experiments were carried out with wall conditioning consisting of boronization and between-shot Helium Glow Discharge cleaning; discharges from these experiments will be referred to as "unlithiated". More recently, NSTX has employed between-shots lithium conditioning of the vessel walls through evaporation from two "LITERs" (LIThium EvapoRators) mounted at the top of the NSTX vessel [6]. Discharges from these experiments will be referred to as "lithiated". Lithium conditioning has led to both lower collisionalities and to improvements in energy confinement time during the H-mode, most notably in the electron channel [7, 8]. It is found that the unlithiated and lithiated discharges scale differently with engineering parameters, but that these differing dependences can be reconciled by an underlying collisionality variation, which unifies both

sets of data and which exhibits a strong improvement of normalized energy confinement with decreasing $\nu^*$. This underlying dependence could potentially influence the design and construction of an ST-based Fusion Nuclear Science Facility (FNSF) [9, 10] strongly, as this class device will operate at collisionalities at least one order of magnitude lower than the operating range of NSTX in this parameter.

## 2. Datasets and Global Confinement Dependences

The discharges used for this study are all H-modes based on $I_p$, $B_T$ scans in both lithiated and unlithiated plasmas, and a lithium deposition scan at fixed $I_p$ and $B_T$. The unlithiated discharges covered the range of $I_p$ from 0.7 to 1.1 MA, $B_T$ from 0.35 to 0.55 T, had deuterium neutral beam (NB) heating powers of $\sim$ 4 MW into Lower Single Null (LSN) deuterium plasmas, elongation, $\kappa$, ~2.2 and plasma densities up to $6\times10^{19}$ m$^{-3}$. All of these discharges exhibited small ELMs, which did not affect confinement significantly. The lithiated discharges were obtained from results of several different experiments, all in the LSN configuration [11, 12]. $I_p$ and $B_T$ scans were performed in sets of discharges for which the between-shots lithium evaporation was held to between 90 and 270 mg. These discharges covered the range $I_p$=0.7 to 1.3 MA, $B_T$=0.34 to 0.54 T, $\kappa$~2.3, and had NB heating powers of approximately 3 MW. Another set of discharges was taken from a lithium evaporation scan (Li scan), covering the range from 0 to 1000 mg of lithium evaporated between shots at fixed $I_p$=0.8 MA, $B_T$=0.44 T and $\kappa$=1.8. The NB heating power in this latter set varied from 2.2 to 4.2 MW. While there were repetitive Type I ELMs at low levels of lithium, the ELMs disappeared at higher levels [13]. Confinement and transport levels for the analysis presented here were taken during inter-ELM periods (for lower deposition values), and thus the direct effect of ELMs was removed.

As reported earlier, the unlithiated plasmas exhibited confinement dependences in H-mode plasmas that showed a strong, nearly linear dependence on $B_T$ with a weaker dependence on $I_p$, going as $I_p^{0.4}B_T^{0.9}$ [1-3]. When transformed to dimensionless physics variables, the NSTX confinement scaling showed a strong increase, almost inverse linearly, with decreasing collisionality [3]. The dependences on both the engineering and physics parameters observed in NSTX were also observed on the MAST spherical tokamak [14, 15]. The lithiated discharges on NSTX, however, revealed confinement dependences on $I_p$ and $B_T$ that are dissimilar from the early NSTX observations, but which are similar to those in conventional aspect ratio tokamaks, as embodied in the ITER98y,2 scaling [16], going as $I_p^{0.86}B_T^{0}$ [17].

The dependence of thermal energy confinement and collisionality on the amount of lithium deposition in the Li scan is quite strong, as can be seen in Figs. 1a and b. The thermal energy confinement times are computed by the TRANSP [18, 19] code. As is seen in Fig. 1a, the total thermal energy confinement, $\tau_E$, increases from 25 to 90 ms, and the electron energy confinement time, $\tau_{Ee}$, increases even more strongly, from 20 to over 100 ms, over the range of lithium deposition. The electron and ion collisionality, taken at $x=[\Phi/\Phi_a]^{1/2}=0.7$ where $\Phi$, $\Phi_a$ are toroidal flux locally and at the plasma edge respectively, shows a strong reduction with increasing lithium deposition, as is seen in Fig. 1b. This indicates a strong inverse dependence of confinement time on collisionality.
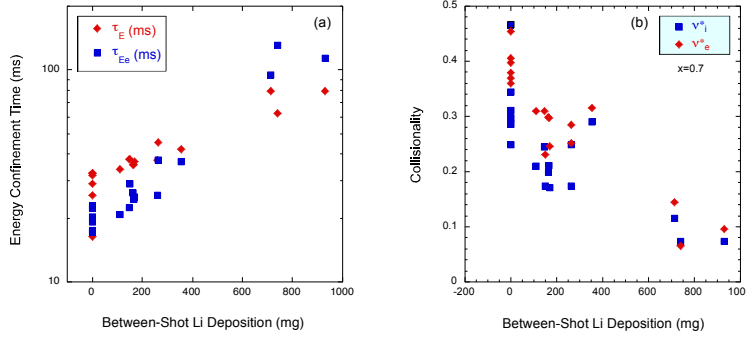
*Fig. 1 (a) Total thermal and electron energy confinement times and (b) ion and electron collisionality as functions of between-shot lithium deposition for the Li scan.*

The relation between $\tau_E$ and collisionality can be readily isolated in the Li scan since engineering parameters, q, $<\beta>$, etc. were held fixed. In the $I_p$ and $B_T$ scans for the lithiated and unlithiated plasmas, however, dimensionless parameters such as q, $<\beta>$ and gyrofrequency $\Omega$ ($\propto 1/B_T$) varied considerably. The $\Omega$ variation has generally been taken into account by normalizing $\tau_E$ by the time

scale given by $\Omega$, which is essentially the same as defining a normalized confinement time, $B_T\tau_E$. Then, the q and $<\beta>$ variations were minimized by choosing a set of discharges within as small a q and $<\beta>$ range as possible, but still having a reasonable number of points to describe the scaling of normalized confinement time with collisionality. This has been done by constraining the data to a $q_{r/a=0.5}$ range of 2 to 2.5 and a $<\beta>$ range of between 8.5 and 12.5%. $\kappa$ was already constrained to 2.2 to 2.4 for these discharges. This set of data, which combines lithiated and unlithiated discharges, gives a factor of four range in collisionality, and it is dubbed the 'Nu scan'. Normalized confinement times for the Nu and Li scans are shown in Figs. 2a and 2b. In Fig. 2a, the lithiated discharges are in red and unlithiated in blue, and it is seen that the normalized confinement time is well-ordered by collisionality (here taken to be the electron collisionality at x=0.5), which unifies the scaling of discharges with



*Fig. 2 Normalized energy confinement time vs collisionality for (a) Nu scan and (b) Li scan*

both types of conditioning. The lithiated discharges generally have lower collisionalities. The overall scaling of this normalized confinement time is strong and favorable as the collisionality decreases ($B\tau_E^{-0.79}$). The same plot for the lithiated discharges (Figs. 1a and 1b) is shown in Fig. 2b, and also shows a similar strong favorable scaling with collisionality ($B\tau_E^{-0.67}$).

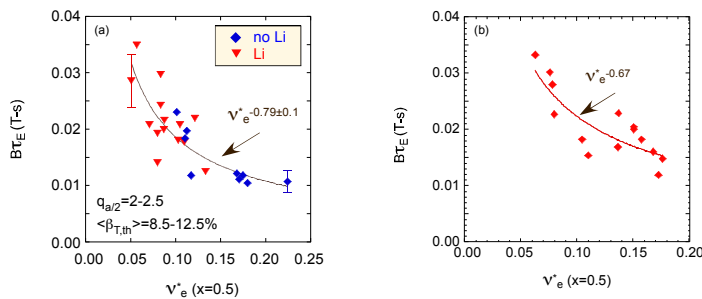The variation of $n_e$, $Z_{eff}$, and $T_e$ in both the Nu and the Li scans was studied to determine which parameter(s) are primarily responsible for variation in $\nu^*$. This study was done for local parameters at x=0.7. For these local studies, a slightly different set of Nu scan discharges were chosen in order to ensure small ranges of both q and $<\beta>$ at that location. It was found that neither the density nor $Z_{eff}$ varied in such a magnitude or fashion to explain the variation in $\nu_e^*$. In fact, $Z_{eff}$ decreased with increasing $\nu_e^*$ for both the Li and the Nu scans, opposite to the expected trend if $Z_{eff}$ was a controlling factor. The factor that influenced the collisionality the most was an increase in local electron temperature resulting from a $T_e$ profile broadening as $\nu_e^*$ decreased, as can be seen in Figs 3a and 3b. As $\nu_e^*$ at x=0.7 decreased from ~0.8 to 0.1, $T_e$ increased at x=0.7 from 250 to 650 eV. The temperature profile peaking factor, defined as $T_e(0)/<T_e>_{vol}$, decreased from ~2.3 to 1.4 for both scans.
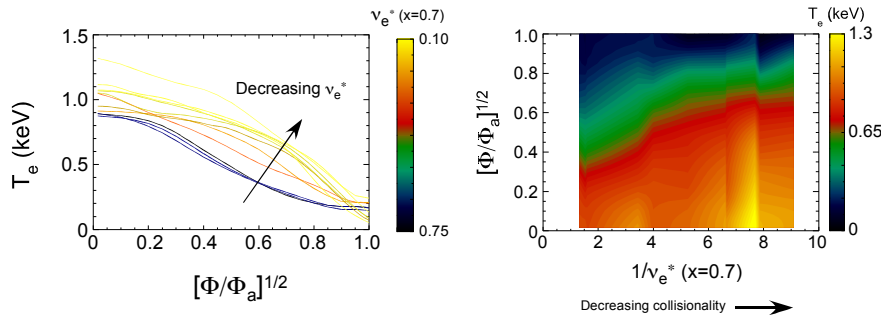
*Fig. 3(a) $T_e$ profiles color coded by collisionality and (b) $T_e$ profile contour plot for the Nu scan.*

One ramification of the change in electron temperature profile is that the dimensionless gyroradius $\rho^*$ is also a strong function of $\nu_e^*$, increasing by a factor of two going from high to low $\nu_e^*$, and the variation of this parameter is expected to influence the confinement time. This variation can be taken into account in the confinement scaling by using the dimensionless scaling $\Omega\tau_E = \rho^{*(-\alpha)} f(\nu,\beta,q,\kappa,...)$ where $\alpha=2$ for Bohm-scaling and $\alpha=3$ for gyroBohm scaling, so that the scalings in Fig. 2 can be recalculated using $\rho^{*\alpha}\Omega\tau_E$ as the independent parameter. The variation of this parameter with $\nu_e^*$ for $\alpha=0$, 2 and 3 is given in Table 1, and it can be seen that because $\rho^*$ increases strongly with decreasing collisionality, the variation is much stronger than for $B\tau_E$ without the $\rho^*$ correction for both scans, especially for the gyroBohm assumption.

TABLE I: COLLISIONALITY DEPENDENCE OF NORMALIZED CONFINEMENT.

|  | $B_T\tau_E$ | $\rho^2 B_T\tau_E$ <br> **Bohm normalization** | $\rho^3 B_T\tau_E$ <br> **gyroBohm normalization** |
|---|---|---|---|
| Nu scan | $\nu_e^{*(-0.79)}$ | $\nu_e^{*(-1.06)}$ | $\nu_e^{*(-1.21)}$ |
| Li scan | $\nu_e^{*(-0.67)}$ | $\nu_e^{*(-1.50)}$ | $\nu_e^{*(-1.91)}$ |

## 3.  Local transport

In this section, the dependences of electron and ion local transport will be discussed, with the ultimate aim of identifying mechanisms believed to be responsible for the transport throughout the range of collisionality being studied. We will focus on the outer region of the plasma ($x \geq 0.6$) since this is the region where changes with changing collisionality are most pronounced. As we saw in Fig. 3a and 3b, the electron temperature increases at $x=0.7$ with decreasing collisionality for both the Nu and Li scans. Indeed, for both scans, a broadening of $T_e$ across the profile, but primarily between $x=0.3$ and 0.9 was observed. This electron temperature profile broadening reflects a progressive reduction in the electron thermal diffusivity in the outer region of the plasma as collisionality decreases. The decrease of the electron thermal diffusivity in the Nu scan can be seen clearly in Fig. 4a. The curves are color-coded to be proportional to the collisionality for that discharge within the collisionality range studied. As can be seen in the figure, the electron thermal diffusivities decrease by approximately an order of magnitude over the range of collisionality at $x=0.7$, going from 10

$m^2/s$ at the highest collisionality to 1 $m^2/s$ at the lowest. The electron thermal diffusivities exhibit the same type of behaviour for the Li scan, but in this scan the difference was even more dramatic, with $\chi_e$ decreasing from 20 $m^2/s$ to 0.7 $m^2/s$ at this location going from the highest to lowest collisionality.
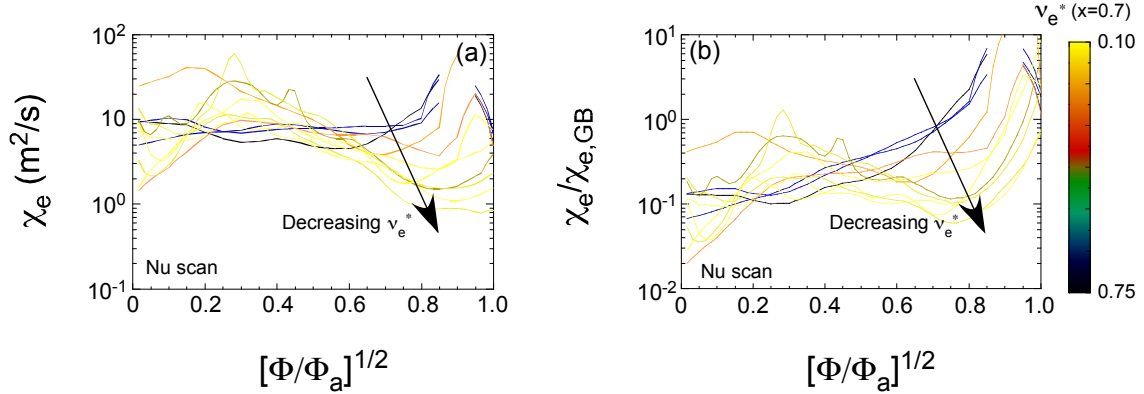


*Fig. 4 (a) Electron thermal diffusivity profiles and (b) $\chi_e$ normalized by $\chi_{e,gyroBohm}$ in arbitrary units color coded by collisionality*

The change in electron thermal diffusivity with collisionality can also be examined in a relative sense by normalizing $\chi_e$ to $\chi_{e,gyroBohm} = \rho^{*2}c_s/a$. This normalization takes into account changes in $\rho^*$ and ion sound speed $c_s$ due to changes in $T_e$ to reflect the transport levels relative to what may be expected by gyroBohm transport. The profiles of $\chi_e/\chi_{e,gyroBohm}$ are shown in Fig. 4b in arbitrary units, and similar to the trend observed for $\chi_e$ alone, the normalized transport also decreases approximately an order of magnitude. A similar result is found for the Li scan as well.

Ion transport behaves differently from that of electrons. Fig. 5a shows the ion thermal diffusivity normalized by the neoclassical ion thermal diffusivity as computed by NCLASS [20] for both scans at x=0.60. This particular radius was chosen for this comparison to avoid regions of sharp gradients in the ion temperature that existed farther out. While there is clearly scatter in the data, $\chi_i/\chi_{i,neo}$ increases approximately a factor of five to ten going from high to low collisionality, a trend that is reversed from that of the electron transport. At the highest collisionality, $\chi_i/\chi_{i,neo} \sim 0.5$, which we take to be at a neoclassical level when the differences among neoclassical theories and the uncertainty in $\chi_i$ (factor of 2) are taken into account. As collisionality decreases, the ions become more anomalous, with $\chi_i/\chi_{i,neo}$ reaching a factor of four to five.

Coupled to this increase in relative ion transport at low collisionality are the trends that both the local toroidal flow velocity increases and



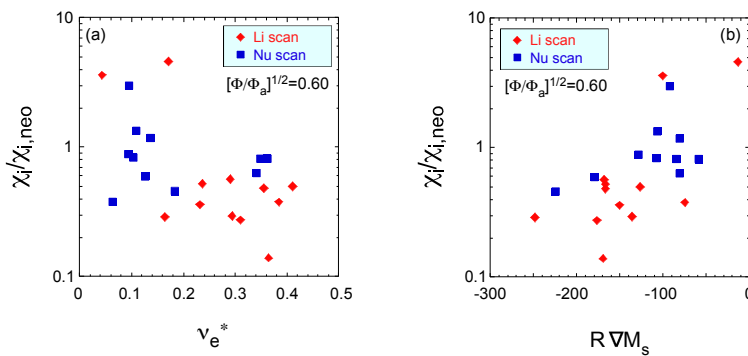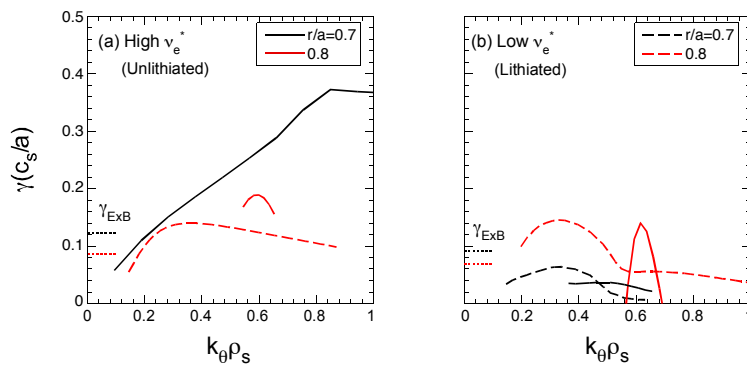*Fig. 5 Ion thermal diffusivity normalized to that from NCLASS neoclassical as a function of (a) collisionality and (b) toroidal flow shear at x=0.6*

toroidal flow shear decreases as collisionality decreases. This is due to a relative broadening in the toroidal flow velocity profiles at this location as collisionality decreases. Fig. 5b shows the relation between the normalized ion transport and the flow shear, as characterized by the normalized gradient of the toroidal Mach number $M_s$. As can be seen, as the flow shear tends toward zero, the normalized ion transport increases; this occurs at low collisionality. This trend may reflect the role of flow shear ($E_r x B$ shear) in suppressing low-k turbulence that can drive anomalous ion transport in NSTX, as observed in earlier analysis of another set of discharges [21].

## 4.  Linear gyrokinetic results

It has been shown previously that both low-k microtearing modes and high-k ETG modes are candidates for driving the anomalous electron energy transport outside the very core region of NSTX plasmas [22-24]. In particular, microtearing has dominated in high-β plasmas [21], while ETG modes tend to be more important at low- β [23, 24]. While the discharges used in these studies qualify as high-β, the strength of both microtearing and ETG modes as a function of collisionality will be investigated. One simple way of assessing the relevance of ETG modes is to compare the electron temperature gradient to the critical gradient for ETG destabilization [25]. While the critical gradient formulation was developed for high aspect ratio, it was shown to be a good indicator for ETG destabilization even in the low aspect ratio NSTX [23]. The $T_e$ profile gradients, as characterized by $R/L_{Te}$, normalized to the critical gradient (also in terms of $R/L_e$) exhibits approximately a factor of five reduction with decreasing collisionality near x=0.7 in the Li scan, decreasing from near 10 to near 1. Farther in, the ratio <1 (indicating stability to ETG modes) and farther out the ratio remains near 1. For the Nu scan, the ratio actually increases with decreasing collisionality near x=0.7; however, the ratio is <1, indicating stability to ETG modes. Farther in, the ratio decreases by approximately one order of magnitude to values <1. These results are borne out by the results of linear gyrokinetic calculations [26], which indicate that for both the Nu and Li scans, the ETG growth rates decrease with decreasing collisionality, with the ETG becoming completely stable at the lowest $v_e^*$.



The results of linear gyrokinetic calculations for low wavenumbers in representative low (lithiated) and high (unlithiated) collisionality discharges from the Nu scan is shown in Figs. 6a and 6b. The results for r/a=0.7, 0.8 (x=0.6, 0.7) are shown. Previous analysis

*Fig. 6 Normalized growth rates of low-k modes from linear GYRO runs for (a) high and (b) low collisionality cases in the Nu scan. The solid lines represent microtearing modes while the dashed lines represent the hybrid TEM/KBM mode. The normalized ExB shearing rates for each radius are given by the color-coded horizontal dashed lines on the left of each plot.*

results for unlithiated discharges alone have shown that microtearing modes were an important component of the electron transport at these wavenumbers, and the decrease in electron transport going from high to low collisionality was associated with the stabilization of the microtearing modes [22]. The results in both the Nu and Li scans support this conclusion, and broadens it by considering the variation of collisionality across the lithiated discharges. Fig.

6a and 6b shows that the microtearing modes (solid lines) are strong and dominant, and much greater than the normalized ExB shearing rate, at the high collisionality at r/a=0.7, but they are completely suppressed at r/a=0.7, however, at the lowest $\nu_e^*$. Some residual microtearing remains at r/a=0.8. On the other hand, the unstable region of the ion modes (dashed curves), actually expands in radius going from high to low collisionality, although both at r/a=0.7 and 0.8, the normalized growth rates are comparable to the normalized ExB shearing rates. The ion modes in this region of the plasma have been identified as hybrid TEM/KBM modes, and will be discussed more in [26]. The increased importance of these ion scale modes is consistent with the increase in anomalous ion transport going from high to low collisionality.

This general result is seen also for the Li scan (Fig. 7a and 7b), although with some more subtlety. The microtearing mode at r/a=0.7 (solid black line) is seen to persist both at high and low collisionality. In fact, its normalized growth rate is much lower relative to the normalized ExB shearing rate in the high than in the low collisionality case (where the two are nearly comparable). So, the microtearing may 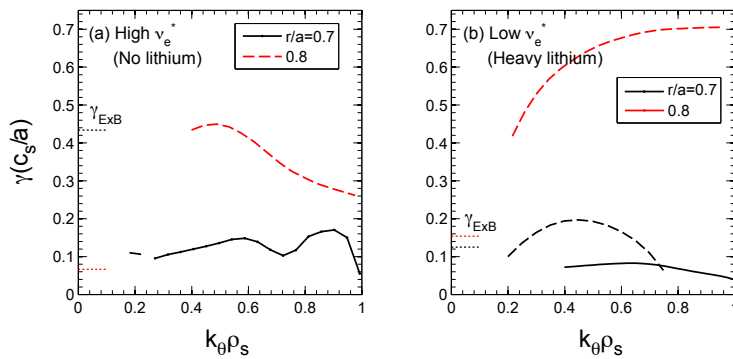still play somewhat of a role in the electron transport in this scan, although non-linear calculations are underway to assess the level of transport induced by these modes. The ion modes, similar to those in the Nu scan (Fig. 6), exhibit increased growth and an expanded region of instability going from the high to the low collisionality case, again consistent with the increase in the level of anomalous ion transport in this scan as well. Here too, non-linear calculations are underway to assess the level of transport induced by these modes.



*Fig. 7 Normalized growth rates of low-k modes from linear GYRO runs for (a) high and (b) low collisionality cases in the Li scan. The solid lines represent microtearing modes while the dashed lines represent the hybrid TEM/KBM mode. The normalized ExB shearing rates for each radius are given by the color-coded horizontal dashed lines on the left of each plot.*

## 5.  Summary

Collisionality has been found to be the unifying parameter in understanding the confinement trends in both unlithiated and lithiated plasmas, with the normalized confinement exhibiting a strong and favourable scaling with decreasing $\nu_e^*$ when holding most other global dimensionless variables (q, β) fixed or limiting their range as much as possible. Folding in the variation of $\rho^*$ actually makes the confinement dependence even stronger when either Bohm or gyroBohm transport is assumed. The reduction in transport at low collisionality is primarily due to an improvement in the electron channel, as reflected by a broadening of the electron temperature profile going from high to low collisionality. ETG modes become completely suppressed at low $\nu_e^*$, and microtearing modes exhibit a reduced extent of instability. The reduction in electron transport more than compensates for an increase in the anomalous ion transport, apparently due to the growth and expansion of a hybrid TEM/KBM mode in the outer region of the plasma at low collisionality. Extrapolating these results to even lower collisionalities representative of ST-based FNSFs is difficult, but will be addressed in experiments on NSTX-Upgrade. It will be important to understand whether the electron

transport will continue to improve as collisionality is further reduced, as well as understanding the role of the ion modes at lower $\nu_e^*$. Whether it is collisionality that controls how anomalous the ion transport is, or whether the ion transport level is tied more tightly to the $E_r$x$B$ shear, will be explored in NSTX-U with its multi-aiming NBI and flexibility to control rotation and rotational shear.

## References

[1]    KAYE, S.M., et al., Nucl. Fusion **46** (2006) 848.

[2]    KAYE, S.M., et al., Phys. Rev Lett. **98** (2007) 175002.

[3]    KAYE, S.M., et al., Nucl. Fusion **47** (2007) 499.

[4]    CONNOR, J.W., Plasma Phys. Controlled Fusion **30** (1988) 619.

[5]    PETTY, C.C., Phys. Plasmas **15** (2008) 080501.

[6]    KUGEL, H.W., et al., Journ. Nucl. Materials **390** (2009) 1000.

[7]    BELL, M.G., et al., Plasma Phys. Controlled Fusion **51** (2009) 124054.

[8]    DING, S., et al., Plasma Phys. Controlled Fusion **52** (2010) 015001.

[9]    MENARD, J.E., et al., Nucl. Fusion **51** (2011) 103014.

[10]   PENG, Y.K.M., et al., Fusion Science and Technology **60** (2011) 441.

[11]   MAINGI, R., et al., Phys. Rev. Lett. **107** (2011) 145004.

[12]   MAINGI, R. et al., Nucl. Fusion **52** (2012) 083001.

[13]   MAINGI, R., et al., Phys. Rev. Lett. **103** (2009) 075001.

[14]   VALOVIC, M., et al., Nucl. Fusion **49** (2009) 075016.

[15]   VALOVIC, M., et al., Nucl. Fusion **51** (2011) 075045.

[16]   ITER Physics Basis, Nucl. Fusion **39** (1999) 2137.

[17]   GERHARDT, S.P., et al., Nucl. Fusion **51** (2011) 073031.

[18]   HAWRYLUK, R.J., et al., in Physics of Plasmas Close to Thermonuclear Conditions: Proceedings Course (Varenna 1979) **1** (1980) 19.

[19]   PANKIN, A., et al., Computer Physics Communications **159** (2004) 157.

[20]   HOULBERG, W.A., et al., Phys. Plasmas **4** (1997) 3230.

[21]   KAYE, S.M., W. Solomon, R.E. Bell, et al., Nucl. Fusion **49** (2009) 045010.

[22]   GUTTENFELDER, W., et al., Phys. Rev. Lett. **106** (2011) 155004.

[23]   MAZZUCATO, E., et al., Phys. Rev. Lett. **101** (2008) 075001.

[24]   REN, Y., et al., Phys. Rev. Lett. **106** (2011) 165005.

[25]   JENKO, F., et al., Phys. Plasmas **8** (2001) 4096.

[26]   GUTTENFELDER, W., et al., Paper EX/7-2, this conference (2012).